Xie *et al. Energy Mater.* **2025**, *5*, 500127
**DOI:** 10.20517/energymater.2025.48

**Energy Materials**

**Article**

**Open Access**



# High-performance Bi-Sb-Te thermoelectric materials synthesized via melt spinning and spark plasma sintering for energy harvesting applications

**Yu-Kun Xie, Settu Ramki, Hsiao-ping Hsu, Chung-Wen Lan***

Crystal Growth Lab, Department of Chemical Engineering, National Taiwan University, Taipei City 10617, Taiwan.

***Correspondence to:** Dr. Chung-Wen Lan, Crystal Growth Lab, Department of Chemical Engineering, National Taiwan University, Da'an District, Taipei City 10617, Taiwan. E-mail:cwlan@ntu.edu.tw

**How to cite this article:** Xie, Y. K.; Ramki, S.; Hsu, H. p.; Lan, C. W. High-performance Bi-Sb-Te thermoelectric materials synthesized via melt spinning and spark plasma sintering for energy harvesting applications. *Energy Mater.* **2025**, *5*, 500127. https://dx.doi.org/10.20517/energymater.2025.48

**Received:** 27 Feb 2025 **First Decision:** 18 Apr 2025 **Revised:** 1 May 2025 **Accepted:** 9 May 2025 **Published:** 26 Jun 2025

**Academic Editors:** Sining Yun, Sung Son Jae **Copy Editor:** Fangling Lan **Production Editor:** Fangling Lan

## Abstract

$Bi_2Te_3$-based materials remain among the most promising thermoelectric candidates for applications in the temperature range of 300-400 K, owing to their high electrical conductivity, low thermal conductivity, chemical stability, and compatibility with scalable fabrication methods. However, conventional crystal growth techniques often lead to elemental segregation and compositional inhomogeneity. In this study, a rapid solidification approach using melt spinning was employed to mitigate segregation, yielding compositionally uniform $Bi_2Te_3$-based powders with particle sizes below 30 μm and nanometer-scale grain structures. The fabrication process - integrating planetary ball milling, annealing, melt spinning, and spark plasma sintering - significantly enhanced phonon scattering, thereby reducing thermal conductivity and improving overall material homogeneity. By systematically adjusting the tellurium content in $Bi_{0.5}Sb_{1.5}Te_{3-x}$, the composition with x = 0.15 was identified as optimal, achieving a peak dimensionless figure of merit (ZT) of 1.18 at 360 K.

**Keywords:** Bismuth telluride, high-temperature silicon-based materials, low-temperature $Bi_2Te_3$, $Bi_{0.5}Sb_{1.5}Te_{3-x}$ (x = 0.15), melt-spinning

## INTRODUCTION

Thermoelectric materials, capable of converting heat into electricity and vice versa, have become essential in

applications such as waste heat recovery, solid-state cooling, and remote power generation. Their operation is governed by the Seebeck and Peltier effects, which facilitate the construction of solid-state thermal devices without moving parts. Compared to conventional thermal engines, thermoelectric systems offer notable advantages, including environmental friendliness, high reliability, and low maintenance requirements, rendering them highly suitable for long-term and sustainable applications[1,2].

Thermoelectric materials are typically classified according to their optimal operating temperature ranges. High-temperature materials, such as silicon-based alloys (e.g., SiGe, $FeSi_2$, and $Mg_2Si$), are employed in harsh or extreme environments. Mid-temperature chalcogenides, including PbTe and SnSe, are well-suited for industrial-scale applications. In contrast, low-temperature materials - particularly $Bi_2Te_3$ and its alloys - exhibit the highest efficiency near room temperature and are widely utilized in applications such as solid-state cooling and small-scale power generation[3,4]. Among these, $Bi_2Te_3$-based compounds are especially notable for their superior thermoelectric performance in the low-temperature regime[5].

Bismuth telluride ($Bi_2Te_3$)-based compounds represent one of the most extensively utilized classes of thermoelectric materials within the near-room-temperature range of 300-400 K, primarily due to their favorable combination of high electrical conductivity and inherently low thermal conductivity. Furthermore, these materials exhibit good chemical stability, can be synthesized with relative ease, and are compatible with large-scale manufacturing processes. As a result of these desirable attributes, $Bi_2Te_3$-based materials are widely implemented in applications such as solid-state refrigeration and the recovery of low-grade waste heat.

Traditional crystal growth techniques often lead to compositional segregation, resulting in material non-uniformity and diminished thermoelectric efficiency[6]. To address this issue, rapid solidification methods - such as atomization and melt-spinning - have been developed to produce powders with uniform chemical composition and nanoscale microstructures[7-9]. Among these, atomization enables rapid cooling, yielding fine powders (< 30 μm) with homogeneous elemental distribution. These powders can then be consolidated into dense thermoelectric materials via sintering techniques such as spark plasma sintering (SPS)[10]. The resulting nanoscale grains significantly enhance phonon scattering, thereby reducing lattice thermal conductivity and improving overall thermoelectric performance.

Although variations in melt-spun ribbon thickness occur due to different copper wheel speeds, previous studies have shown that ribbon thickness does not significantly affect thermoelectric properties, including electrical conductivity, Seebeck coefficient and the dimensionless figure of merit (ZT)[11,12]. This suggests that even when ribbon thickness deviates from literature-reported values, the thermoelectric performance remains largely unaffected. In our prior experiments, varying the duration of planetary ball milling revealed that a milling time of 10 h produced the most homogeneous composition. Furthermore, the incorporation of melt-spinning was found to be crucial, as evidenced by X-ray diffraction (XRD) results. Samples subjected to melt-spinning exhibited sharper and more distinct peaks, indicating improved phase purity and crystallinity, thereby highlighting the importance of this step in thermoelectric material synthesis.

Elemental composition also plays a significant role in optimizing thermoelectric performance. Increasing antimony content was observed to enhance electrical conductivity; however, it also led to a reduction in the Seebeck coefficient, ultimately lowering the power factor. Conversely, reducing tellurium content increased electrical conductivity while slightly decreasing the Seebeck coefficient. Nevertheless, the overall ZT value improved within the temperature range of 423-523 K, indicating that tellurium vacancies may contribute

positively to thermoelectric performance by optimizing the carrier concentration and enhancing phonon scattering[13].

In this study, $Bi_{0.5}Sb_{1.5}Te_{3-x}$ was selected as the benchmark material for the development of high-performance thermoelectric alloys. Our findings demonstrate that reducing tellurium content from x = 0 to x = 0.15 significantly enhances thermoelectric properties. This composition adjustment achieves a better balance between carrier concentration and lattice thermal conductivity, retaining high electrical conductivity and a relatively high Seebeck coefficient while promoting phonon scattering. As a result, a maximum ZT value of approximately 1.15 at 360 K was obtained, indicating excellent energy conversion efficiency.

Due to the volatility of tellurium during the melt-spinning process, an annealing step was introduced prior to rapid solidification. This thermal treatment stabilizes tellurium and prevents undesirable structural degradation or decomposition during processing, thereby preserving the integrity of the final material. The inclusion of annealing not only enhances phase stability but also improves the overall thermoelectric performance and reliability of the resulting alloys.

Therefore, we adopted an integrated synthesis strategy comprising planetary ball milling, annealing, melt-spinning, elemental compensation and SPS. Planetary ball milling facilitates uniform mixing and grain refinement, thereby enhancing phonon scattering. Annealing stabilizes the tellurium content by minimizing volatilization and suppressing structural transformations. Melt-spinning induces rapid solidification, promoting uniform microstructure formation. Finally, SPS enables rapid densification with minimal grain growth, preserving the nanoscale features essential for high thermoelectric efficiency[14,15].

## EXPERIMENTAL

### Materials synthesis

*Synthesis of $Bi_{0.5}Sb_{1.5}Te_{3-x}$*

High-purity elemental powders of bismuth (Bi, 99.999%, 5N), antimony (Sb, 99.999%, 5N), and tellurium (Te, 99.999%, 5N) were used as starting materials. The powders were weighed according to the nominal composition of $Bi_{0.5}Sb_{1.5}Te_{3-x}$, with varying Te contents to investigate the effect of Te deficiency. The weighed powders were loaded into a zirconia ball milling jar under an argon atmosphere and subjected to high-energy mechanical alloying using a planetary ball mill. The milling was conducted at a rotational speed of 450 rpm for 10 h, with a ball-to-powder weight ratio of 20:1.

The mechanically alloyed powders were subsequently annealed at 627 K for 10 h in order to relieve internal stress and promote phase formation. The annealed powders were then loaded into a quartz nozzle with an inner diameter of 0.4 mm for the melt-spinning process. A rotating copper wheel with a surface speed of approximately 39.3 m/s (3,000 rpm) was employed to rapidly solidify the molten alloys, forming nanostructured ribbons of $Bi_{0.5}Sb_{1.5}Te_{3-x}$.

To compensate for potential elemental losses during melt spinning, energy-dispersive X-ray spectroscopy (EDS) analyses were performed on the ribbons to assess and adjust the final composition toward the target stoichiometry. The as-spun ribbons were pulverized into fine powders and consolidated using SPS (SPS-515S, SYNTEX INC) at 753 K under an applied uniaxial pressure of 50 MPa for three minutes. The sintered pellets had a diameter of 23 mm and a thickness of approximately 5 mm.

### Materials characterizations

XRD (Rigaku MiniFlex) for SPSed pellets was performed on parallel and perpendicular planes of SPS pressing direction. The microstructure was analyzed by scanning electron microscopy (SEM, JEOL JSM-

5310) in low vacuum mode for enhanced imaging quality and detail. The temperature dependence of electrical conductivity and Seebeck coefficients was measured from 300 to 482 K using a commercially available instrument (ZEM-3, ULVAC-RIKO, Japan) apparatus, ensuring precise thermal and transport property analysis. The specimen size is typically parallel piped with the dimensions of 5 × 5 × 15 $mm^3$. The thermal conductivity values of the pellet specimen with a dimension of 2 mm in thickness and 23 mm in diameter measured from 300 to 482 K were measured by hot disk (TPS 3500). Based on the above data, we can obtain the ZT value through calculation. Figure 1 shows the schematic diagram of experimental process. First, we begin with planetary ball milling synthesis, followed by annealing and melt spinning. Since element loss can occur during the melt spinning process, we perform EDS measurements after melt spinning to determine the elemental composition and compensate to achieve the desired stoichiometry. Finally, we proceed with SPS.

## RESULTS AND DISCUSSION

The XRD patterns presented in Figure 2 provide comprehensive insights into the structural evolution of $Bi_{0.5}Sb_{1.5}Te_3$ under various synthesis and processing conditions. Figure 2A compares samples subjected to three different treatments: 3-h ball milling (3h-BM), 10-h ball milling (10h-BM), and 10-h ball milling followed by 10-h annealing (10h-BM + AN). The 3h-BM sample displays broad and less intense diffraction peaks, indicative of poor crystallinity. This can be attributed to inadequate mechanical activation and smaller grain sizes due to the shorter milling duration. In contrast, the 10h-BM sample exhibits significantly sharper and more intense peaks, suggesting enhanced crystallinity facilitated by extended milling, which promotes more uniform grain formation and better particle refinement. Subsequent annealing of the 10h-BM sample (10h-BM + AN) further sharpens the diffraction peaks and improves their alignment with the standard reference pattern (JCPDS 00-49-1713)[16], confirming improved phase purity and crystallite growth. This observation highlights the synergistic effect of prolonged mechanical alloying and thermal treatment in enhancing the structural quality of $Bi_{0.5}Sb_{1.5}Te_3$. Considering the temperature-sensitive nature of tellurium and its propensity for phase transitions, improper thermal control can lead to the formation of undesirable phases during melt spinning. The annealing step thus plays a critical role in stabilizing the crystalline structure before subsequent processing, mitigating abrupt phase changes and promoting controlled structural evolution.

Figure 2B further elucidates the influence of melt spinning and tellurium (Te) content variation on the structural characteristics of $Bi_{0.5}Sb_{1.5}Te_3$. Four processing routes are examined BST-BM + AN + SPS, BST-BM + AN + MS + SPS, BST-BM + AN + MS + SPS (with 15 wt% additional Te), and BST-BM + AN + MS + SPS (with 25 wt% additional Te). The BST-BM + AN + SPS sample shows well-resolved diffraction peaks corresponding to the $Bi_{0.5}Sb_{1.5}Te_3$ phase, indicating successful crystallization. The introduction of a melt spinning step (BST-BM + AN + MS + SPS) further enhances the peak intensity and sharpness, reflecting improved crystallinity and finer grain refinement. The addition of Te during processing, especially at 25 wt%, results in even more pronounced diffraction peaks. This suggests that excess Te plays a role in stabilizing the $Bi_{0.5}Sb_{1.5}Te_3$ phase and suppressing the formation of structural defects or secondary phases[17,18]. These results emphasize the critical importance of both processing technique and compositional tuning in optimizing the microstructural properties of thermoelectric materials[19,20].

Prolonged ball milling, annealing and melt spinning collectively contribute to the enhancement of crystallinity in $Bi_{0.5}Sb_{1.5}Te_3$, as evidenced by the emergence of sharper and more intense XRD peaks. Notably, samples subjected to melt spinning exhibit significantly more pronounced diffraction peaks compared to those processed without this step, indicating a substantial improvement in crystal structure refinement. In contrast, samples prepared with shorter processing durations or without post-treatment display broader and

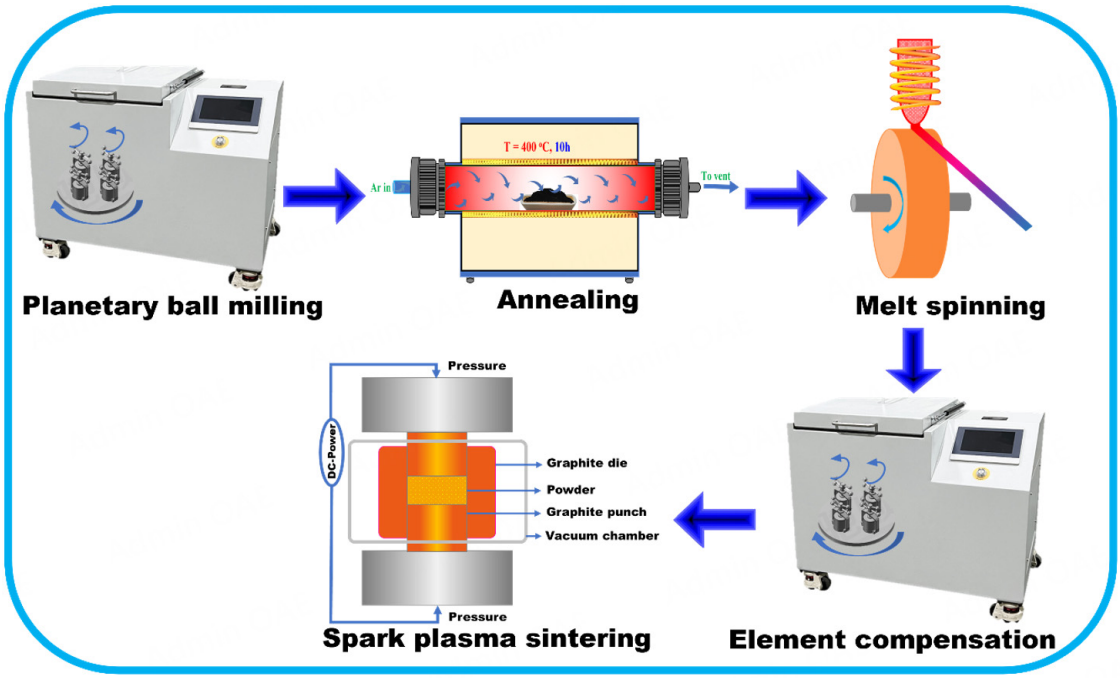


**Figure 1.** The schematic diagram of experimental process.

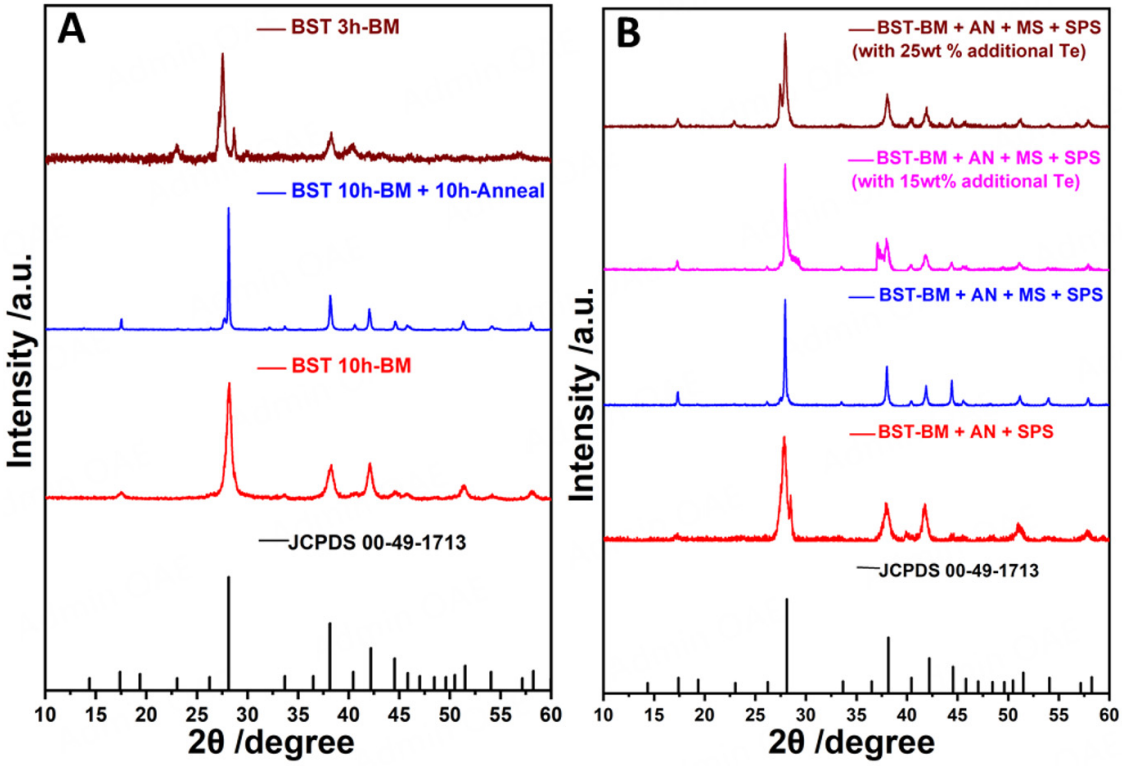


**Figure 2.** (A) X-ray diffraction (XRD) patterns of $Bi_{0.5}Sb_{1.5}Te_3$ powders synthesized under varying ball milling durations, with and without post-synthesis annealing, illustrating the influence of mechanical processing and thermal treatment on phase composition. (B) XRD patterns of polycrystalline $Bi_{0.5}Sb_{1.5}Te_3$ bulks obtained from melt-spun ribbons, highlighting the structural differences between samples processed with and without the melt-spinning technique.

less intense peaks, suggesting reduced crystallinity and the presence of smaller grain sizes. These observations underscore the critical importance of synthesis strategies and compositional control in optimizing the crystalline structure of $Bi_{0.5}Sb_{1.5}Te_3$. The combined effects of extended ball milling, thermal annealing, melt spinning and appropriate elemental compensation play a pivotal role in improving the structural integrity of the material, thereby laying the foundation for enhanced thermoelectric performance.

Traditionally, thermoelectric materials have been synthesized through ball milling followed by SPS. In contrast, the present study employs a modified approach involving ball milling followed by melt spinning. This method allows for more precise control over the material's microstructure and results in improved uniformity compared to conventional ball milling alone. Ball milling and melt spinning are fundamentally different techniques, each yielding distinct microstructural features due to their inherent processing mechanisms.

As illustrated in Figure 3A and B, ball milling is a high-energy mechanical process that subjects material particles to repeated fracturing, cold welding and re-fracturing. It is widely utilized for particle refinement, homogenization and alloying purposes[21,22]. Typically, ball milling yields nanocrystalline grains in the range of 10 to 100 nm, attributed to severe plastic deformation and dynamic recrystallization[23]. The process also introduces a high density of lattice defects, such as dislocations, grain boundaries and vacancies, which can significantly enhance atomic diffusion and facilitate phase transformations. With extended milling durations, ball milling can promote atomic-scale homogenization, resulting in solid solutions or finely dispersed composite structures. In certain cases, it may even induce amorphization by disrupting long-range atomic order[24]. The resultant particles generally exhibit irregular morphologies and broad particle size distributions. The specific microstructural characteristics are largely dependent on parameters such as milling duration, impact energy and the intrinsic properties of the starting materials.

Figure 3C and D depicts the annealing treatment employed prior to melt spinning, which is essential to minimize tellurium (Te) volatilization during subsequent processing. Figure 3E and F highlights the microstructural features produced by melt spinning, a rapid solidification technique that offers several advantages over ball milling. One of the primary benefits is the extremely high cooling rates on the order of $10^5$ to $10^6$ K/s which enable the formation of amorphous or metastable phases that are difficult to achieve through mechanical milling[25]. This rapid quenching process promotes superior compositional uniformity by suppressing phase segregation and facilitating the retention of homogenous microstructures[26,27]. Compared to the time-intensive and mechanically demanding ball milling process, melt spinning is both faster and more energy-efficient. Additionally, it reduces the risk of contamination and excessive defect formation, which are often associated with repeated mechanical collisions in ball milling.

Furthermore, melt spinning is particularly effective for producing thin ribbons or films with smooth, continuous surfaces, in contrast to the irregularly shaped particles typically obtained from ball milling. These attributes make melt spinning a favorable technique for fabricating advanced functional materials, especially in applications that require controlled microstructures, such as magnetic alloys, amorphous metals and high-performance thermoelectric or coating materials[28].

Figure 4A shows a SEM image revealing the microstructure of the sample. A specific region of interest, marked by a pink box, indicates the area selected for further elemental analysis. A yellow cross within the region denotes the precise location where Energy-Dispersive X-ray Spectroscopy (EDS) was performed. Figure 4B displays the elemental mapping of tellurium (Te), represented in green. The mapping reveals a relatively uniform distribution of Te throughout the analyzed region, suggesting that Te is a well-

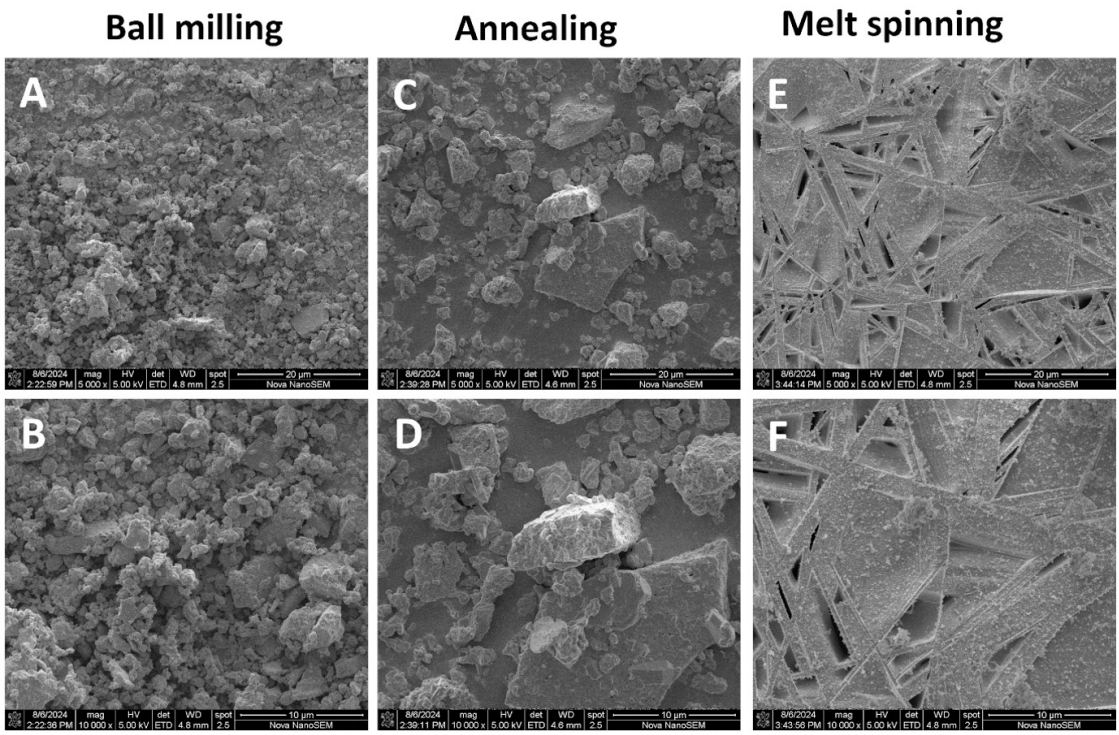


**Figure 3.** Microstructural evolution of $Bi_{0.5}Sb_{1.5}Te_{3-x}$ observed at different processing stages (A and B) after ball milling, (C and D) following annealing, and (E and F) post melt-spinning. These images reveal the effects of each process on particle morphology, grain refinement and structural homogeneity.

incorporated and essential constituent of the material matrix. Figure 4C shows the elemental distribution of antimony (Sb), indicated in yellow. Sb appears to be the dominant element and exhibits a strong spatial overlap with Te, implying a homogeneous integration within the same phase. Figure 4D presents the mapping of bismuth (Bi), represented in red. Bi is also uniformly distributed and exhibits considerable spatial correlation with both Sb and Te. The collective results from these elemental maps indicate that the sample is composed of a Bi-Sb-Te ternary alloy, a system widely known for its thermoelectric properties and its ability to efficiently convert thermal energy into electrical energy. The observed uniform distribution of Bi, Sb, and Te across the selected region further suggests a well-mixed and homogeneous microstructure, which is critical for optimizing charge carrier transport and minimizing phonon scattering in thermoelectric materials[29,30].

The SEM micrograph presented in the top-left section of Figure 5 provides a cross-sectional view of the sample. Captured at a magnification of 4,000×, the image reveals a distinct layered morphology with sharp, well-defined interfaces, indicative of a potentially crystalline structure. The total thickness of the sample is approximately 53.91 μm, as indicated by the green vertical scale marker. Five specific locations, labeled points 1 through 5, are marked within the layered region, presumably as reference sites for subsequent compositional or elemental analysis. Figure 5A-D displays elemental distribution maps acquired via EDS, illustrating the spatial distribution of key elements within the cross-section of the sample. These maps reveal a uniform dispersion of the constituent elements across the examined region. The observed compositional homogeneity is essential for functional materials, particularly in thermoelectric applications, where consistent elemental distribution contributes to stable electrical and thermal transport properties.

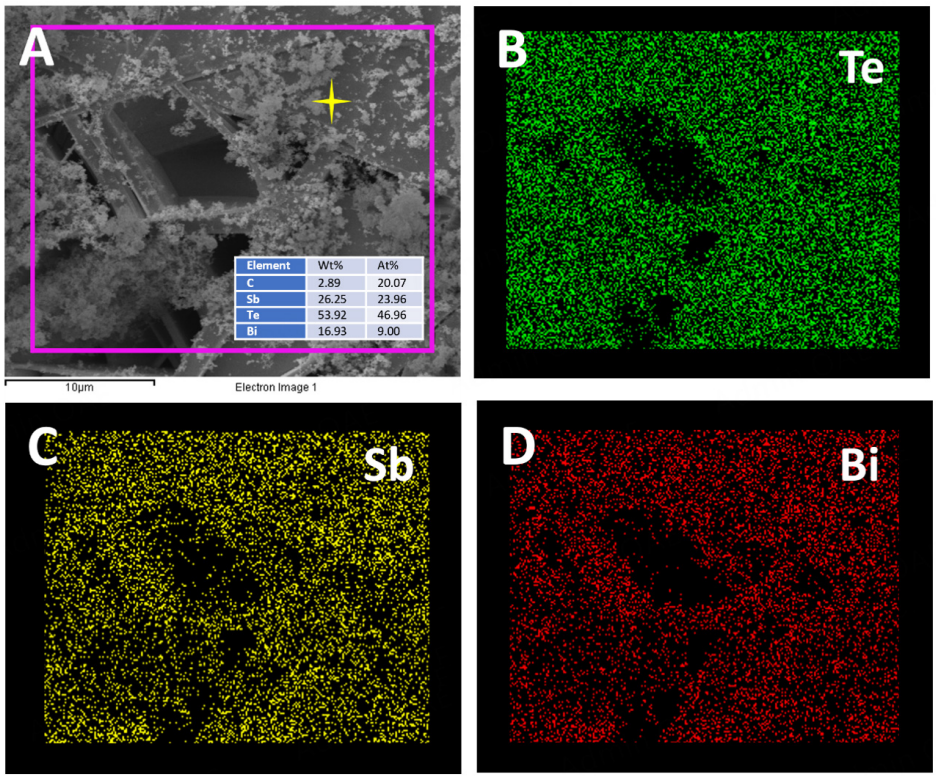


**Figure 4.** Energy-dispersive X-ray spectroscopy (EDS) elemental mapping of $Bi_{0.5}Sb_{1.5}Te_{3-x}$. (A) Top-view SEM image of the melt-spun ribbon, with corresponding elemental distribution maps of (B) tellurium, (C) antimony and (D) bismuth, confirming a homogeneous spatial distribution of the constituent elements.

Figure 6A and B, labeled "Ribbon Composition" and located at the bottom of the image, presents quantitative data on the elemental composition at the five designated points within the SEM cross-sectional image. The analysis reveals that bismuth (Bi, shown in red), tellurium (Te, green), and antimony (Sb, blue) are the predominant elements, maintaining consistent proportions across all five measured locations. Figure 7A-D further supports these findings, reinforcing the conclusion that the sample comprises a ternary alloy system, most likely based on Bi-Sb-Te. The uniform elemental distribution and compositional consistency observed across the sample suggest that the material is well-integrated and homogenous in nature. Such characteristics are critical for thermoelectric materials, particularly $Bi_2Te_3$-based alloys, which are widely recognized for their high efficiency in converting thermal gradients into electrical energy. The combination of Bi, Sb and Te in a stable and uniformly distributed microstructure indicates that the material is engineered for optimal thermoelectric performance. These alloys are commonly employed in power generation and solid-state cooling technologies due to their favorable electrical conductivity and low thermal conductivity[31,32].

Overall, the data presented in these figures provide compelling evidence that the sample possesses a layered structure with excellent compositional homogeneity. These features strongly support its potential application in high-performance thermoelectric devices. Further characterization, including thermal conductivity, Seebeck coefficient and electrical resistivity measurements is recommended to fully evaluate the material's suitability for practical energy conversion applications[33].

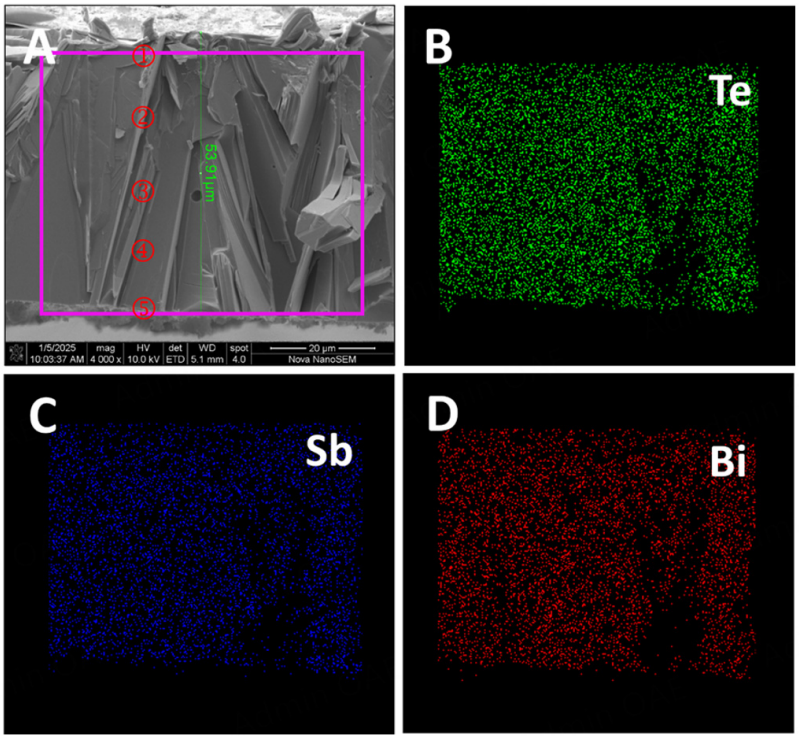


**Figure 5.** Cross-sectional energy-dispersive X-ray spectroscopy (EDS) mapping of $Bi_{0.5}Sb_{1.5}Te_{3-x}$ melt-spun ribbon. (A) Cross-sectional SEM image, with corresponding elemental distribution maps of (B) tellurium, (C) antimony and (D) bismuth, demonstrating uniform elemental dispersion across the ribbon thickness.

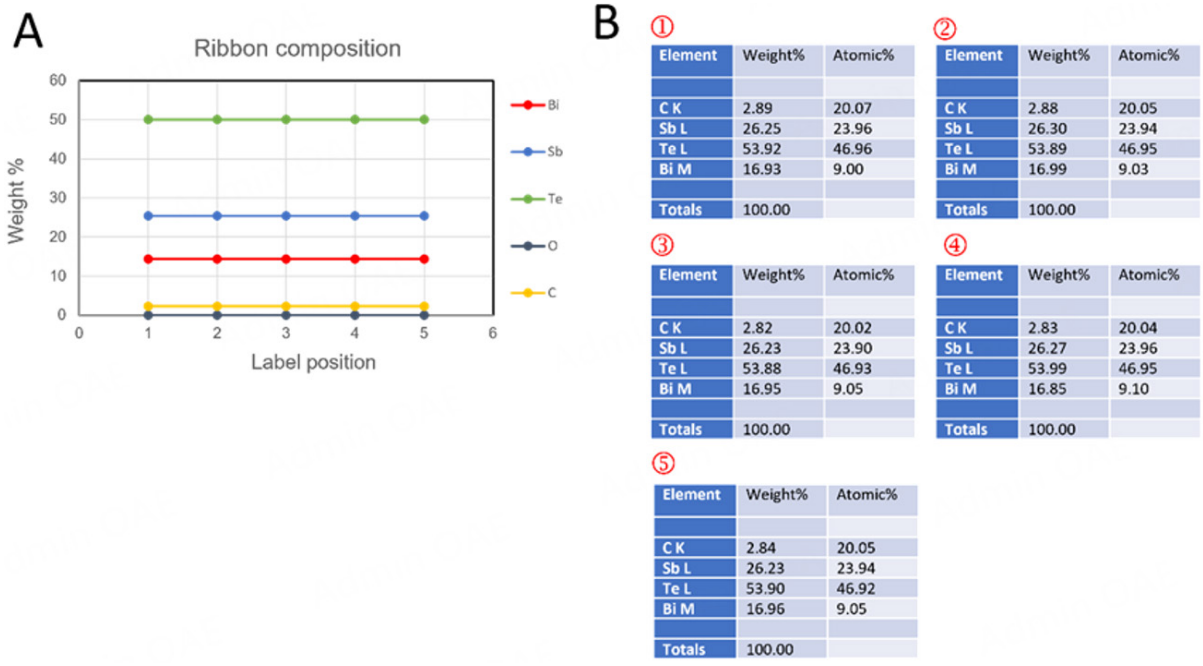


**Figure 6.** (A) Elemental distribution across the cross-section of a $Bi_{0.5}Sb_{1.5}Te_{3-x}$ melt-spun ribbon, illustrating compositional uniformity at various positions. (B) Corresponding EDS spectra acquired from selected regions, confirming consistent elemental composition throughout the cross-section.

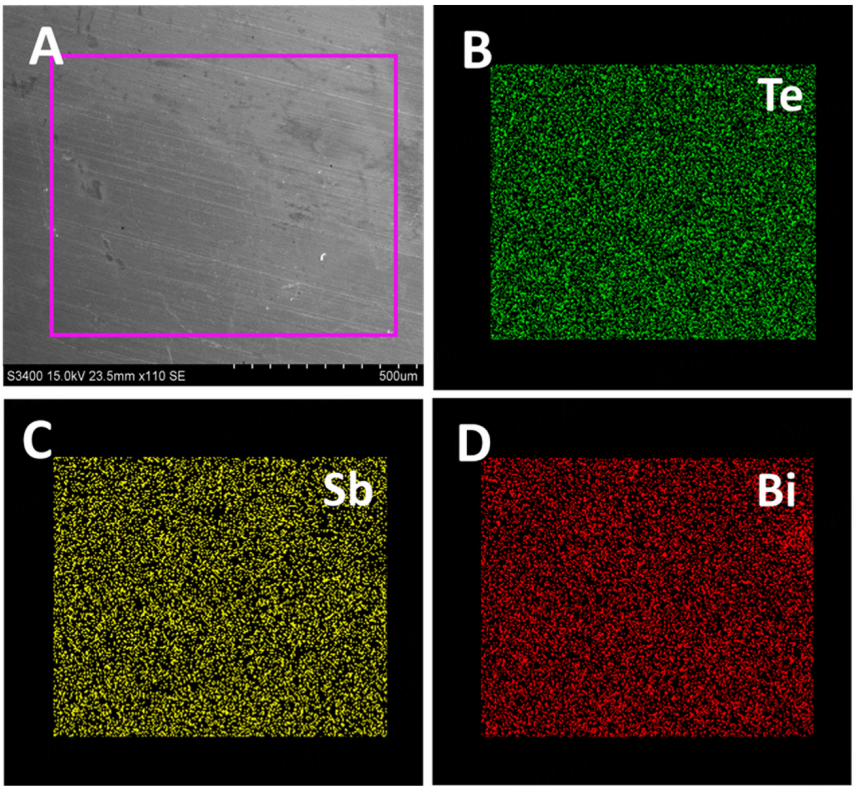


**Figure 7.** Energy-dispersive X-ray spectroscopy (EDS) mapping of $Bi_{0.5}Sb_{1.5}Te_{3-x}$ spark plasma sintered (SPS) pellet. (A) Top-view SEM image of the pellet surface, with corresponding elemental distribution maps of (B) tellurium, (C) antimony and (D) bismuth, indicating a uniform elemental distribution across the surface.

In this study, the thermoelectric properties of melt-spun Bi-Sb-Te compounds with varying compositions (x = 0.15, x = 0, and x = -0.15) were systematically investigated over a temperature range of 300-480 K. The primary thermoelectric parameters analyzed include electrical conductivity (σ), the Seebeck coefficient, and the power factor. Among these, electrical conductivity is a crucial factor, as it directly influences the efficiency of thermoelectric energy conversion[34,35]. Figure 8A illustrates the temperature-dependent electrical conductivity of the Bi-Sb-Te samples. For the composition with x = 0.15, the electrical conductivity at room temperature (300 K) was measured to be 1,046 $S \cdot cm^{-1}$. As the temperature increased to 480 K, the conductivity decreased to 739 $S \cdot cm^{-1}$. In comparison, the samples with x = 0 and x = -0.15 exhibited lower electrical conductivities at room temperature, measured at 392 and 346 $S \cdot cm^{-1}$, respectively. Across all compositions, electrical conductivity was observed to decrease with increasing temperature, a behavior consistent with degenerate semiconductor characteristics[36]. These results indicate that carrier scattering increases with temperature, leading to a reduction in mobility and, consequently, a decline in electrical conductivity. The higher σ value observed in the x = 0.15 sample suggests improved carrier concentration or mobility, potentially due to optimal stoichiometry or microstructural features induced by the melt spinning process.

A significant enhancement in electrical conductivity was achieved by reducing the Te content in Bi-Sb-Te compounds. Specifically, the conductivity increased from 392.25 $S \cdot cm^{-1}$ for $Bi_{0.5}Sb_{1.5}Te_{3-x}$ (x = 0) to 1,046.87 $S \cdot cm^{-1}$ for $Bi_{0.5}Sb_{1.5}Te_{3-x}$ (x = 0.15). This improvement is primarily attributed to the formation of antisite defects induced by Te deficiency, which generates a higher hole concentration, as confirmed by Hall carrier concentration measurements. Among the tested compositions, the x = 0.15 sample consistently

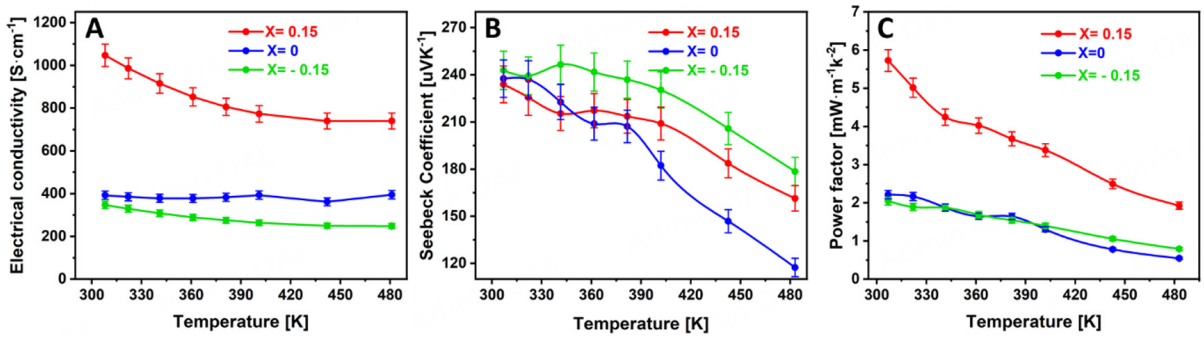


**Figure 8.** Temperature-dependent thermoelectric properties of $Bi_{0.5}Sb_{1.5}Te_{3-x}$ samples (A) electrical conductivity (B) Seebeck coefficient and (C) power factor. These results highlight the influence of tellurium content on the thermoelectric performance over the measured temperature range.

exhibited the highest electrical conductivity, indicating enhanced charge carrier mobility and favorable microstructural characteristics[37].

In contrast, the x = 0 and x = -0.15 compositions demonstrated significantly lower conductivity values. This suggests that these compositions may suffer from increased defect densities, phase separation, or microstructural disorder, which hinder effective charge transport[38,39]. The observed decrease in electrical conductivity with increasing temperature for all compositions is typical of degenerate semiconductors, where thermal excitation leads to enhanced carrier scattering and reduced mobility[40]. The superior conductivity of the x = 0.15 sample may be attributed to an optimized microstructure that promotes continuous and efficient charge transport pathways.

The Seebeck coefficient (S), a measure of the thermoelectric voltage generated in response to a temperature gradient, is shown in Figure 8B for all three compositions. The Seebeck coefficient values are positive across the measured temperature range, indicating that the $Bi_{0.5}Sb_{1.5}Te_{3-x}$ compounds are p-type semiconductors[41]. All samples exhibited an increase in S with temperature, reaching a peak near 340 K before declining at higher temperatures. This trend is characteristic of thermoelectric semiconductors, where charge carrier mobility and carrier concentration interact dynamically with thermal excitation.

At room temperature, the Seebeck coefficient values were 233 $\mu V \cdot K^{-1}$ for x = 0.15, 237 $\mu V \cdot K^{-1}$ for x = 0 and 242 $\mu V \cdot K^{-1}$ for x = -0.15. Notably, the x = 0.15 sample maintained the highest Seebeck coefficient across the entire temperature range, suggesting that this composition is most effective at generating thermoelectric voltage. A high Seebeck coefficient is desirable for thermoelectric applications as it enhances the material's ability to convert thermal energy into electrical energy.

Figure 8C presents the temperature dependence of the power factor ($PF = S^2\sigma$) for the three $Bi_{0.5}Sb_{1.5}Te_{3-x}$ samples. At room temperature, the x = -0.15 composition exhibited the lowest PF of 2.04 $mW \cdot m^{-1} \cdot K^{-2}$ due to its poor electrical conductivity. Conversely, the x = 0.15 sample demonstrated the highest PF of 5.72 $mW \cdot m^{-1} \cdot K^{-2}$. For all compositions, the power factor initially increased with temperature, reaching a maximum before declining slightly at higher temperatures.

The x = 0.15 composition consistently outperformed the other two in terms of power factor, indicating a superior balance between electrical conductivity and Seebeck coefficient. This makes it the most promising candidate among the three for high-performance thermoelectric applications. Given that the power factor is

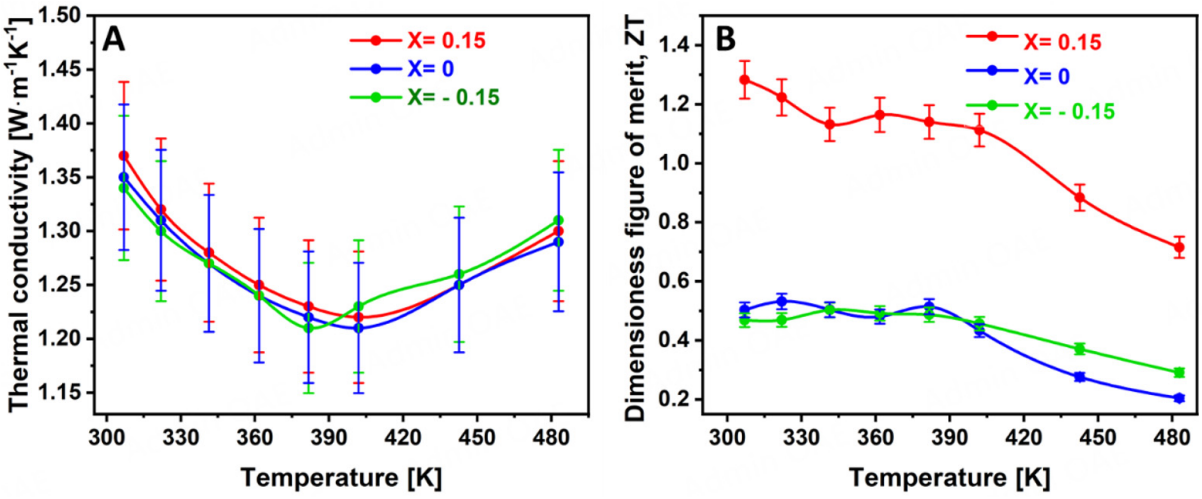


**Figure 9.** Temperature-dependent thermoelectric performance of $Bi_{0.5}Sb_{1.5}Te_{3-x}$ samples (A) total thermal conductivity and (B) dimensionless figure of merit. The data illustrate the effect of tellurium deficiency on thermal transport properties and overall thermoelectric efficiency.

a critical component of the thermoelectric ZT, the enhanced PF of the x = 0.15 sample strongly suggests its suitability for efficient energy conversion systems[42].

Thermal conductivity (κ), another essential parameter for thermoelectric performance, was measured over a temperature range of 300-480 K, as shown in Figure 9A. The data reveal a general decrease in κ with increasing temperature for all three compositions (x = 0.15, 0, -0.15). This behavior is desirable for thermoelectric materials, as reduced thermal conductivity at elevated temperatures helps maintain a large temperature gradient across the material, thereby improving energy conversion efficiency.

Figure 9B presents the dimensionless ZT as a function of temperature for $Bi_{0.5}Sb_{1.5}Te_{3-x}$ samples with three different compositions: x = 0.15, x = 0, and x = -0.15. The ZT value is a critical indicator of thermoelectric performance, incorporating contributions from electrical conductivity, Seebeck coefficient, and thermal conductivity. Generally, an increase in ZT with temperature suggests enhanced thermoelectric efficiency at elevated temperatures.

Among the three compositions, the sample with x = 0.15 exhibited the highest ZT value, reaching approximately 1.18 at 360 K. This significant improvement highlights the beneficial effect of Te vacancies on thermoelectric performance. The presence of tellurium vacancies likely promotes the formation of antisite defects, enhancing carrier concentration and optimizing the balance between electrical and thermal transport properties. Therefore, compositional tuning through Te reduction proves to be an effective strategy for improving the thermoelectric performance of Bi-Sb-Te-based materials.

## CONCLUSIONS

This study reports the successful synthesis of homogeneous $Bi_{0.5}Sb_{1.5}Te_{3-x}$ thermoelectric materials via melt spinning followed by SPS. To address the challenges associated with compositional segregation commonly observed in conventional crystal growth techniques, atomization and melt spinning were employed. These rapid solidification methods facilitate the formation of powders with uniform composition and refined nanoscale grain structures, which are advantageous for enhancing thermoelectric performance upon subsequent densification by SPS.

The optimized composition with x = 0.15 exhibited superior thermoelectric properties, achieving a maximum dimensionless ZT of approximately 1.18 at 360 K. The synergistic integration of rapid solidification, nanostructuring, and compositional optimization offers an effective strategy for the development of high-performance thermoelectric materials. This approach not only mitigates issues such as phase segregation and excessive grain coarsening inherent in traditional synthesis methods but also presents a viable route for advancing thermoelectric materials in energy conversion and solid-state cooling applications.

## DECLARATIONS

### Authors' contributions

Made substantial contributions to conception and design of the study and performed data collection and visualization: Xie, Y. K.; Ramki, S.; Lan, C. W. H

Performed data acquisition and provided administrative, technical, and material support: Xie, Y. K.; Ramki, S.; Hsu, H. p.

### Availability of data and materials

The data are made available upon request to authors.

### Financial support and sponsorship

This work was supported by the National Science and Technology Council of Taiwan [112-2221-E-002-039-MY3].

### Conflicts of interest

All authors declared that there are no conflicts of interest.

### Ethical approval and consent to participate

Not applicable.

### Consent for publication

Not applicable.



## REFERENCES

1. He, J.; Tritt, T. M. Advances in thermoelectric materials research: looking back and moving forward. *Science* **2017**, *357*, eaak9997. DOI PubMed
2. Yang, L.; Chen, Z.; Dargusch, M. S.; Zou, J. High performance thermoelectric materials: progress and their applications. *Adv. Energy. Mater.* **2018**, *8*, 1701797. DOI
3. Cao, T.; Shi, X.; Li, M.; et al. Advances in bismuth-telluride-based thermoelectric devices: progress and challenges. *eScience* **2023**, *3*, 100122. DOI
4. Goldsmid, H. J. Bismuth telluride and its alloys as materials for thermoelectric generation. *Materials* **2014**, *7*, 2577-92. DOI PubMed PMC
5. Mamur, H.; Bhuiyan, M.; Korkmaz, F.; Nil, M. A review on bismuth telluride ($Bi_2Te_3$) nanostructure for thermoelectric applications. *Renew. Sustain. Energy. Rev.* **2018**, *82*, 4159-69. DOI
6. Zharikov, E. V. Problems and recent advances in melt crystal growth technology. *J. Cryst. Growth.* **2012**, *360*, 146-54. DOI
7. Hegde, G. S.; Prabhu, A. N. A review on doped/composite bismuth chalcogenide compounds for thermoelectric device applications: various synthesis techniques and challenges. *J. Electron. Mater.* **2022**, *51*, 2014-42. DOI
8. Xie, W.; Tang, X.; Yan, Y.; Zhang, Q.; Tritt, T. M. Unique nanostructures and enhanced thermoelectric performance of melt-spun BiSbTe alloys. *Appl. Phys. Lett.* **2009**, *94*, 102111. DOI
9. Zheng, Y.; Xie, H.; Zhang, Q.; et al. Unraveling the critical role of melt-spinning atmosphere in enhancing the thermoelectric

performance of p-type $Bi_{0.52}Sb_{1.48}Te_3$ alloys. *ACS. Appl. Mater. Interfaces.* **2020**, *12*, 36186-95. DOI
10. Han, L.; Spangsdorf, S. H.; Nong, N. V.; et al. Effects of spark plasma sintering conditions on the anisotropic thermoelectric properties of bismuth antimony telluride. *RSC. Adv.* **2016**, *6*, 59565-73. DOI
11. Shin, W. H.; Yoon, J. S.; Jeong, M.; et al. Microstructure analysis and thermoelectric properties of melt-spun Bi-Sb-Te compounds. *Crystals* **2017**, *7*, 180. DOI
12. Zhang, Q.; Zhang, Q.; Chen, S.; et al. Suppression of grain growth by additive in nanostructured p-type bismuth antimony tellurides. *Nano. Energy.* **2012**, *1*, 183-9. DOI
13. Qin, H.; Qu, W.; Zhang, Y.; et al. Nanotwins strengthening high thermoelectric performance bismuth antimony telluride alloys. *Adv. Sci.* **2022**, *9*, e2200432. DOI PubMed PMC
14. Poudel, B.; Hao, Q.; Ma, Y.; et al. High-thermoelectric performance of nanostructured bismuth antimony telluride bulk alloys. *Science* **2008**, *320*, 634-8. DOI
15. Xie, W.; Wang, S.; Zhu, S.; et al. High performance $Bi_2Te_3$ nanocomposites prepared by single-element-melt-spinning spark-plasma sintering. *J. Mater. Sci.* **2013**, *48*, 2745-60. DOI
16. Hu, L.; Zhu, T.; Wang, Y.; Xie, H.; Xu, Z.; Zhao, X. Shifting up the optimum figure of merit of p-type bismuth telluride-based thermoelectric materials for power generation by suppressing intrinsic conduction. *NPG. Asia. Mater.* **2014**, *2*, e88. DOI
17. Xie, W.; Zhu, B.; Wu, X.; Cao, W.; Wang, Z. Synergistic strategy for enhancing the thermoelectric properties of $Bi_{0.5}Sb_{1.5}Te_3$ with excess Te through low-temperature liquid phase sintering method. *J. Eur. Ceram. Soc.* **2024**, *44*, 5765-73. DOI
18. Kim, E. B.; Dharmaiah, P.; Lee, K.; et al. Enhanced thermoelectric properties of $Bi_{0.5}Sb_{1.5}Te_3$ composites with in-situ formed senarmontite $Sb_2O_3$ nanophase. *J. Alloys. Compd.* **2019**, *777*, 703-11. DOI
19. Kim, D. H.; Kim, T.; Lee, S. W.; Kim, H. S.; Shin, W. H.; Kim, S. I. Investigation of phase segregation in p-Type $Bi_{0.5}Sb_{1.5}Te_3$ thermoelectric alloys by in situ melt spinning to determine possible carrier filtering effect. *Materials* **2021**, *14*, 7567. DOI PubMed PMC
20. Kim, H.; Kim, T.; An, J.; Kim, D.; Jeon, J. H.; Kim, S. Segregation of $NiTe_2$ and $NbTe_2$ in p-type thermoelectric $Bi_{0.5}Sb_{1.5}Te_3$ alloys for carrier energy filtering effect by melt spinning. *Appl. Sci.* **2021**, *11*, 910. DOI
21. Dwivedi, S. P.; Saxena, A.; Sharma, S.; et al. Effect of ball-milling process parameters on mechanical properties of $Al/Al_2O_3$/collagen powder composite using statistical approach. *J. Mater. Res. Technol.* **2021**, *15*, 2918-32. DOI
22. Shang, X.; Wang, X.; Chen, S. Effects of ball milling processing conditions and alloy components on the synthesis of Cu-Nb and Cu-Mo alloys. *Materials* **2019**, *12*, 1224. DOI PubMed PMC
23. El-Eskandarany, M.; Mahday, A. A.; Ahmed, H.; Amer, A. Synthesis and characterizations of ball-milled nanocrystalline WC and nanocomposite WC-Co powders and subsequent consolidations. *J. Alloys. Compd.* **2000**, *312*, 315-25. DOI
24. Yang, Y.; Sun, W.; Fang, Q.; Yuan, Z. Effect of ball milling nanocrystallization on hydrogen storage performance of $Mg_{95}Ni_2Pr_3$ hydrogen storage alloy. *Mater. Today. Commun.* **2024**, *40*, 109380. DOI
25. Ciftci, N.; Ellendt, N.; Coulthard, G.; Soares, B. E.; Mädler, L.; Uhlenwinkel, V. Novel cooling rate correlations in molten metal gas atomization. *Metall. Mater. Trans. B.* **2019**, *50*, 666-77. DOI
26. Arun, S.; Radhika, N.; Saleh, B. Advances in vacuum arc melting for high entropy alloys: a review. *Vacuum* **2024**, *226*, 113314. DOI
27. Wen, J.; Cheng, J.; Min, X.; Huang, Y.; Liu, Y. Strengthened solid solution and homogenized eutectic structure of Al-based multi-component alloy via electromagnetic stirring. *J. Alloys. Compd.* **2024**, *1002*, 175537. DOI
28. Vishwakarma, A.; Chauhan, N. S.; Bhardwaj, R.; et al. Melt-spun SiGe nano-alloys: microstructural engineering towards high thermoelectric efficiency. *J. Electron. Mater.* **2021**, *50*, 364-74. DOI
29. Du, B.; Wu, J.; Lai, X.; et al. Fabrication and electrical properties of $Bi_{2-x}Sb_xTe_3$ ternary nanopillars array films. *Ceram. Int.* **2019**, *45*, 3244-9. DOI
30. Li, J. W.; Han, Z.; Yu, J.; et al. Wide-temperature-range thermoelectric n-type $Mg_3(Sb, Bi)_2$ with high average and peak zT values. *Nat. Commun.* **2023**, *14*, 7428. DOI PubMed PMC
31. Yen, W.; Huang, H.; Wang, K.; Wu, H. Nano-precipitation and carrier optimization synergistically yielding high-performance n-type $Bi_2Te_3$ thermoelectrics. *Mater. Today. Phys.* **2021**, *19*, 100416. DOI
32. Wu, H.; Yen, W. High thermoelectric performance in Cu-doped $Bi_2Te_3$ with carrier-type transition. *Acta. Mater.* **2018**, *157*, 33-41. DOI
33. Zhuang, H.; Pei, J.; Cai, B.; et al. Thermoelectric performance enhancement in BiSbTe alloy by microstructure modulation via cyclic spark plasma sintering with liquid phase. *Adv. Funct. Mater.* **2021**, *31*, 2009681. DOI
34. Zhang, X.; Zhao, L. Thermoelectric materials: energy conversion between heat and electricity. *J. Materiomics.* **2015**, *1*, 92-105. DOI
35. Hamid, E. M.; Shnawah, D. A.; Sabri, M. F. M.; et al. A review on thermoelectric renewable energy: principle parameters that affect their performance. *Renew. Sustain. Energy. Rev.* **2014**, *30*, 337-55. DOI
36. Yang, J.; Wang, Z.; Zhao, H.; et al. Effect of composition adjustment on the thermoelectric properties of $Mg_3Bi_2$-based thermoelectric materials. *Micromachines* **2023**, *14*, 1844. DOI PubMed PMC
37. Jin, S.; Ziabari, A.; Koh, Y. R.; et al. Enhanced thermoelectric performance of p-type $Bi_xSb_{2-x}Te_3$ nanowires with pulsed laser assisted electrochemical deposition. *Extreme. Mech. Lett.* **2016**, *9*, 386-96. DOI
38. Choi, H.; Kim, S. J.; Kim, Y.; We, J. H.; Oh, M.; Cho, B. J. Enhanced thermoelectric properties of screen-printed $Bi_{0.5}Sb_{1.5}Te_3$ and $Bi_2Te_{2.7}Se_{0.3}$ thick films using a post annealing process with mechanical pressure. *J. Mater. Chem. C.* **2017**, *5*, 8559-65. DOI
39. Liu, W.; Hong, T.; Cheng, X.; et al. Alloy scattering to optimize carrier and phonon transport properties in $PbBi_2S_4$ thermoelectric. *J.*

*Materiomics.* **2025**, *11*, 100938. DOI

40. Cui, J.; Xue, H.; Xiu, W.; Mao, L.; Ying, P.; Jiang, L. Crystal structure analysis and thermoelectric properties of p-type pseudo-binary $(Al_2Te_3)_x$-$(Bi_{0.5}Sb_{1.5}Te_3)_{1-x}$ (x= 0~0.2) alloys prepared by spark plasma sintering. *J. Alloys. Compd.* **2008**, *460*, 426-31. DOI
41. Cooley, J. A.; Promkhan, P.; Gangopadhyay, S.; et al. High Seebeck coefficient and unusually low thermal conductivity near ambient temperatures in layered compound $Yb_{2-x}$ $Eu_xCdSb_2$. *Chem. Mater.* **2018**, *30*, 484-93. DOI
42. Dehkordi A, Zebarjadi M, He J, Tritt TM. Thermoelectric power factor: enhancement mechanisms and strategies for higher performance thermoelectric materials. *Mater. Sci. Eng. R. Rep.* **2015**, *97*, 1-22. DOI